



Enhance Displacement Amplification Ratio of Micro-Gripper Compliant Mechanisms Using Bridge-Type Amplifier Based on Make a Decision Criteria and Grey-Taguchi Method

Nguyen Ho¹, Ngoc Thai Huynh², Quoc Manh Nguyen³, Minh Hue Pham Thi⁴, The Vinh Do^{5*}

¹ Faculty of Electrical and Electronics Engineering, Ton Duc Thang University, Ho Chi Minh City 700000, Vietnam

² Faculty of Mechanical Engineering Technology, Ho Chi Minh City University of Industry and Trade, Ho Chi Minh City 700000, Vietnam

³ Faculty of Mechanical Engineering, Hung Yen University of Technology and Education, Khoai Chau, Hung Yen 160000, Vietnam

⁴ School of Mechanical and Automotive Engineering, Hanoi University of Industry, Hanoi 100000, Vietnam

⁵ Faculty of Mechanical Engineering, Thai Nguyen University of Technology, Thai Nguyen city, Thai Nguyen 250000, Vietnam

Corresponding Author Email: thevinh8880@tnut.edu.vn

Copyright: ©2024 The authors. This article is published by IETA and is licensed under the CC BY 4.0 license (<http://creativecommons.org/licenses/by/4.0/>).

<https://doi.org/10.18280/mmep.111124>

ABSTRACT

Received: 15 June 2024

Revised: 19 August 2024

Accepted: 30 August 2024

Available online: 29 November 2024

Keywords:

micro gripper compliant mechanisms, flexure hinge, optimization, grey-Taguchi, WASPAS, TOPSIS, VIKOR

Creating a compliant mechanism that has a high displacement amplification ratio, a large workspace, low stress, and a high frequency is difficult. Thus, this paper used SolidWorks to design the gripper mechanisms using the series bridge-type (BT) compliant mechanism. Minitab software was used to create orthogonal arrays for the study. The finite element method (FEM) in ANSYS was used to analyze displacement and equivalent stress of the studying model. The Taguchi method was used to evaluate the influence of design variables. The grey relational analysis (GRA) method with MEREC weighting method was utilized to maximize displacement and minimize principal stress. In this investigation, the designed dimension consisted of the thickness of the flexure hinge (FH) was from 0.2 to 0.4 mm, the length of the FH increased from 3 mm to 4 mm, the distance between the centers of the two FHs changed from 0.8 mm to 1.2 mm depending on each position, and the radius between the rigid link and FHs increased from 0.4 to 0.8 mm. The outcomes of the FEM and analysis of signal-to-noise (S/N) of all of the models showed that the designed dimension had significant influenced on the displacement magnification ratio of the micro-gripper compliant mechanism. With an input displacement of 0.01 mm, the optimal displacement and equivalent stress were obtained at 0.62241 mm and 121.08 MPa, respectively, by the grey relational analysis. The optimal case is the third case, with the thickness of the FH was 0.2 mm, the length of the FH was 3 mm, the distance between the centers of the two flexure hinges was 1.2 mm, and the radius between the rigid link and flexure hinges was 0.8 mm. The make a decision criteria consisted of TOPSIS, SAW, WASPAS, and VIKOR techniques, all demonstrate that the third case was the best.

1. INTRODUCTION

To replace conventional joints, researchers have created a variety of flexible hinges (FH) [1]. Compliant mechanisms are preferred for displacement amplification because of their benefits, which include vacuum compatibility, no assembly, no friction, no lubrication, and no rebound. The mechanics using common materials have good applications in the fields of medicine and soft robotics [2]. This is demonstrated by experiments and FEM analysis in ANSYS. The resonance frequency of the micro-gripper was improved based on the pseudo-stiffness and bending beam model [3]. This problem was confirmed by finite element analysis and experimental model. The Piezoelectric material is employed to actuate the microgripper compliant mechanism designed based on bridge-type and lever type [4]. Experiments have confirmed that the

proposed mechanism has high displacement amplification and accurate object folding and releasing. A fully integrated and coupled design method in a smart structure is applied to improve the amplification of the compliant mechanism based on the Topology method [5] and piezoelectric stack actuators. The 3D-PLAST has been applied to improve the limitations in the fabrication of flexure hinges for flexible mechanisms [6]. The experiments also confirmed the high reliability of the design model. To improve the performance of the compliant mechanism, a hybrid bending hinge is developed from elliptical and hyperbolic [7]. The experimental and finite element results show that the performance is significantly improved. The enhanced stick-slip theory and the direct drive theory have been applied to the 3-DOF piezoelectric robot [8]. The experimental results and finite element analysis confirm that the modified stick-slip concept outperforms the original

stick-slip principle in terms of effectiveness. In addition, the robot can carry objects weighing more than 500g. The adjoint method was applied to optimize three design variables simultaneously by speed-based optimization [9]. The piezoelectric actuator was also applied to drive the compliant mechanism. Numerical simulation results show that the piezoelectric actuator can significantly improve the performance of the compliant mechanism. The pseudo rigid is used to improve the displacement amplification of MEMs accelerometer based on displacement amplifier [10]. The finite element analysis results show that the performance of MEMs accelerometer is higher than that of conventional accelerometer. The gripper and flapping wing actuator was fabricated based on the compliant frame [11]. The Experimental results and finite element analysis show that the proposed model avoids multiple assembly and its warping. The proposed model folds the object more efficiently. The compact nanopositioning system with high displacement amplification fabricated with acrylic significantly improved the amplification compared to that fabricated with spring steel [12]. This result was confirmed by experiment and finite element analysis (FEA). The outcomes of this method were contrasted with those of the FEM and its previous research. Micro-gripper-compliant mechanisms (MGCM) that use flexure hinges have been widely popular. The MGCM mechanism used the elastic deformation of the material to control position and force. The MGCM using BT [13] was designed and constructed for testing. Both the FEA and the experimental results, in our opinion, yield excellent results. According to certain publications, grippers only utilized half of the bridge mechanism (BM), resulting in a smaller space occupied. To generate a single or double direction displacement output, the piezoelectric actuator (PZT) was frequently positioned in the center of the BT [14]. The longitudinally positioned BM in the MGCM with BT usually generates double-sided output. The performance of the microgripper compliant mechanism is improved based on the application of parallelogram structure and multi-stage amplifier [15]. The experimental findings demonstrate that the suggested model grasps various copper wires with considerable amplification. The transfer matrix method is applied to the kinematic and dynamic analysis of serial-parallel compliant mechanisms [16]. Timoshenko straight beams are used to validate the theoretical displacement results and numerical simulations. Two bridge amplifiers are used to create a three-dimensional bridge amplifier structure. Lateral stiffness and parasitic displacement are minimized thanks to parallel guide beams [17]. The accuracy and performance of this model are confirmed by experiments and finite element analysis. The L-shaped mechanism and parallelogram mechanism are adopted to improve the clamping stroke of the microgripper [18]. The experimental and numerical simulation results obtained confirm the best outcomes of the response surface method-based model. Coupled the two BT to increase the end-effector stroke. The principle of the lever amplifier is applied to amplify the microgripper compliant mechanism [19]. The optimal parameters and performance of the model are achieved by finite element analysis and experiment. The electromechanical transmission matrix method is applied to improve the actuation performance of amplified piezoelectric actuators [20]. An experiment has been carried out to determine the reliability of the proposed method. The balanced performance and effective clamping of the microgripper system are achieved based on the experimental results of

clamping force and finger displacement [21]. To enhance the functionality of the MGCM. The hybrid gain mechanism has been designed based on the use of 3 different flexure hinge types [22]. The experimental results and finite element analysis achieve reliable performance of the proposed model. The beam element mass matrix, stiffness matrix and elasticity theory have been constructed to improve the dynamic performance of the rotational two-degree-of-freedom and translational one-degree-of-freedom mechanism [23]. To ascertain the computing efficiency of the suggested theoretical model, a dynamic experiment is conducted.

Different from the old study, the gripper mechanism is used in the series BT compliant mechanism (GMSBTCM) to analyze the horizontal displacement gripper. The purpose of this study is for the model's output displacement and stress outputs to outperform earlier studies while the input displacement value remains constant. As a result, the authors employ a variety of optimization techniques to assess the study model fairly and precisely. The differences of this study compared with previous studies are as follows:

- Designed the GMSBTCM by SOLIDWORKS software.
- Minitab 18 generated the L27 orthogonal array.
- Analysis of FEA, displacement, and stress of GMSBTCM by ANSYS software.
- The influence of design variables was evaluated using the Taguchi method's S/N analysis (S/N-A).
- MEREC method was applied to compute the weight measurement technique for the grey relational analysis (Grey-R-A), TOPSIS, SAW, WASPAS, and VIKOR methods.
- Grey-R-A was utilized to calculate the optimal of GMSBTCM on FEA in ANSYS.
- The TOPSIS, SAW, WASPAS, and VIKOR methods confirmed the optimal result.

The rest of the paper is presented as follows: the model of GMSBTCM, FEM, and evaluation of the weight were described in Section 2. Section 3 simulates FEA, analyzes the optimal methods, and compares the results. Finally, Section 4 offers conclusions.

2. CAD MODEL, FINITE ELEMENT ANALYSIS, AND EVALUATE THE WEIGHT

2.1 CAD model

The GMSBTCM was shown in Figure 1, and 27 mechanism models were created using SolidWorks. The GMSBTCM has two BT. The first BT's output was the input for the second BT. The detailed dimensions of GMSBTCM are depicted in Figure 2. The total dimension of GMSBTCM was 92 mm for x-axis, 68 mm for y-axis, and 5 mm for z-axis. The series bridge-type compliant was connected to the gripper body by a flexure hinge as presented in Figure 1 with the length was 1.5 mm, the thickness was 0.4 mm, and the radius was 0.5 mm.

The gripper body was attached to the fixed body of the mechanism by the measurements of a BT are 4 mm in length, 0.4 mm in thickness, and 0.5 mm in radius. The dimensions of the design variables include the L variable, which is the length of the FHs. The D variable is the distance between the centers of the two FHs. The FHs' thickness is the T variable. The R variable is the radius between the rigid link and flexible hinges. The study model was then analyzed using the FEA in ANSYS to determine the study model's values of displacement and maximum principal stress. The FEM and boundary conditions are detailed in Section 2.2.

table of 27 cases to use for this study. The S/N ratio (S/N-R) was used to determine a loss function to calculate the difference between the experiment or simulation and the actual values. The "the larger, the better" (Eq. (1)) and "the smaller, the better" (Eq. (2)) categories were used in this paper.

$$S / N = -10 \log \left(\frac{1}{n} \sum_{i=1}^n \frac{1}{y_i^2} \right) \quad (1)$$

$$S / N = -10 \log \left(\frac{1}{n} \sum_{i=1}^n y_i^2 \right) \quad (2)$$

where, y_i 's variance represents the observed data for each characteristic and n denotes the number of experiments. The Taguchi method and S/N-A were developed in this study using the Minitab 18 software. In order to evaluate how design variables affect model output outcomes, the acquired findings are shown in the outcomes and Discussion section.

2.4 MEREC method

It uses a completely new MCDM algorithm to generate outcomes that are more exact and precise. This method uses the removal effect on the alternative estimation of each criterion to generate the criteria weights. An option's assessment following the criteria's removal that considers deviations is a novel concept in determining criteria weights [26]. Decision-makers may find it simpler to exclude particular criteria from consideration if they adopt this point of view, which also establishes the objective weight of each criterion [27]. The MEREC method was applied to compute the weight for every objective as follows:

Step 1: Determine h_{ij} , the largest value is the optimal in Eq. (3), and the smallest value is optimal in Eq. (4).

$$h_{ij} = \frac{\min u_{ij}}{u_{ij}} \quad (3)$$

$$h_{ij} = \frac{u_{ij}}{\max u_{ij}} \quad (4)$$

u_{ij} are the values of D_i and S_i obtained from the method mentioned in Section 2.2.

Step 2: Determine the total performance of objectives

$$S_i = \ln \left[1 + \left(\frac{1}{n} \sum_j \ln(h_{ij}) \right) \right] \quad (5)$$

Step 3: Determine S'_{ij}

$$S'_{ij} = \ln \left[1 + \left(\frac{1}{n} \sum_{k, k \neq j} \ln(h_{ij}) \right) \right] \quad (6)$$

Step 4: Determine the deviation

$$E_j = |S'_{ij} - S_i| \quad (7)$$

Step 5: Determine the weight of every criterion

$$w_j = \frac{E_j}{\sum_k E_k} \quad (8)$$

3. RESULTS AND OPTIMIZATION METHOD

3.1 Set up simulation

According to the study [1], the displacement and stress are affected by the distance between adjacent FHs, the FHs' length and the connected objects' length, the thickness of the FH, and other structural parameters have low sensitivity. This was also demonstrated by Kee-Bong Choi and colleagues from Korea Institute of Machinery and Materials, South Korea [10]. In this study, the variables were selected as depicted in Figure 2 and listed in Table 1. First, the length of the FH is the L variable along with three levels: 3 mm, 3.5 mm, and 4 mm. Next, the D variable is the distance between the centers of the two FHs; it has three levels: 0.8, 1, and 1.2; its unit is mm. The T variable is the thickness of FHs; it has three levels: 0.2, 0.3, and 0.4; its unit is mm. Finally, the R variable is the radius between the rigid link and flexure hinges; it has three levels: 0.4, 0.6, and 0.8; its unit is mm.

Twenty-seven cases were created with Minitab software, and the SolidWorks software designed twenty-seven models. Then, twenty-seven instances were imported into ANSYS' static structure module to analyze stress and displacement. The FEM was carried out in this module as presented in Section 2.2.

Table 2 depicts the simulation results from ANSYS. The 6th column shows the result of displacements, and the 8th column shows the result stress. According to this table, changing the input variables causes the output position and the stress of the gripper to change with different values in columns 6th, 8th. The results of twenty-seven cases are different, which proves that the input variable has an influence on the results.

Table 1. The factors and their levels

Designed Dimensions	Symbol	Unit	Level 1	Level 2	Level 3
Length of flexure hinge	L	mm	3	3.5	4
Distance between two centers of two flexure hinges	D	mm	0.8	1	1.2
The R variable is the radius between the rigid link and flexure hinges	R	mm	0.4	0.6	0.8
The T variable is the thickness of FHs	T	mm	0.2	0.3	0.4

Table 2. L27 orthogonal array and simulation results

Experiment No.	Thickness (T)	Length (L)	Distance (D)	Radius (R)	Displacement (mm)	S/N of Output Displacement	Stress (MPa)	S/N of Output Stress
1	0.2	3.0	0.8	0.4	0.38462	-8.2994	141.15	-42.9936
2	0.2	3.0	1.0	0.6	0.5195	-5.6883	136.47	-42.7007
3	0.2	3.0	1.2	0.8	0.62241	-4.1185	121.08	-41.6614

4	0.2	3.5	0.8	0.6	0.36112	-8.8470	134.26	-42.5589
5	0.2	3.5	1.0	0.8	0.49519	-6.1046	118.97	-41.5087
6	0.2	3.5	1.2	0.4	0.4115	-7.7126	107.14	-40.5990
7	0.2	4.0	0.8	0.8	0.34113	-9.3416	120.35	-41.6089
8	0.2	4.0	1.0	0.4	0.30407	-10.3405	102.71	-40.2323
9	0.2	4.0	1.2	0.6	0.38162	-8.3674	92.937	-39.3638
10	0.3	3.0	0.8	0.4	0.24418	-12.2458	127.26	-42.0938
11	0.3	3.0	1.0	0.6	0.32682	-9.7138	117.64	-41.4111
12	0.3	3.0	1.2	0.8	0.38457	-8.3005	110.36	-40.8562
13	0.3	3.5	0.8	0.6	0.2356	-12.5565	119.89	-41.5757
14	0.3	3.5	1.0	0.8	0.31567	-10.0153	112.71	-41.0392
15	0.3	3.5	1.2	0.4	0.35072	-9.1008	118.02	-41.4391
16	0.3	4.0	0.8	0.8	0.22741	-12.8638	111.53	-40.9478
17	0.3	4.0	1.0	0.4	0.26593	-11.5047	113.19	-41.0762
18	0.3	4.0	1.2	0.6	0.32219	-9.8378	101.32	-40.1139
19	0.4	3.0	0.8	0.4	0.14326	-16.8775	115.44	-41.2471
20	0.4	3.0	1.0	0.6	0.19292	-14.2925	101.06	-40.0916
21	0.4	3.0	1.2	0.8	0.23223	-12.6816	99.703	-39.9742
22	0.4	3.5	0.8	0.6	0.14128	-16.9984	101.29	-40.1113
23	0.4	3.5	1.0	0.8	0.19181	-14.3426	104.43	-40.3765
24	0.4	3.5	1.2	0.4	0.25053	-12.0228	107.38	-40.6185
25	0.4	4.0	0.8	0.8	0.13885	-17.1491	98.526	-39.8710
26	0.4	4.0	1.0	0.4	0.19232	-14.3195	118.89	-41.5029
27	0.4	4.0	1.2	0.6	0.2349	-12.5823	96.256	-39.6686

Table 3. The values were obtained by the MEREC method

Experiment No.	h_{ij}		S_i	S_{ij}		e_j	
	D_i	S_t		D_i	S_t	D_i	S_t
1	0.3610	1.0000	0.4117	0.0000	0.4117	0.4117	0.0000
2	0.2673	0.9668	0.5168	0.0167	0.5067	0.5000	0.0101
3	0.2231	0.8578	0.6026	0.0739	0.5597	0.5287	0.0429
4	0.3845	0.9512	0.4074	0.0247	0.3906	0.3827	0.0168
5	0.2804	0.8429	0.5431	0.0820	0.4921	0.4610	0.0509
6	0.3374	0.7591	0.5194	0.1291	0.4339	0.3903	0.0856
7	0.4070	0.8526	0.4247	0.0767	0.3712	0.3480	0.0535
8	0.4566	0.7277	0.4388	0.1475	0.3307	0.2913	0.1081
9	0.3638	0.6584	0.5391	0.1898	0.4091	0.3493	0.1300
10	0.5686	0.9016	0.2882	0.0505	0.2486	0.2377	0.0396
11	0.4249	0.8334	0.4181	0.0872	0.3563	0.3309	0.0618
12	0.3611	0.7819	0.4901	0.1160	0.4117	0.3740	0.0784
13	0.5893	0.8494	0.2971	0.0785	0.2346	0.2187	0.0626
14	0.4399	0.7985	0.4208	0.1066	0.3441	0.3142	0.0767
15	0.3959	0.8361	0.4400	0.0857	0.3807	0.3543	0.0594
16	0.6106	0.7902	0.3107	0.1113	0.2205	0.1994	0.0903
17	0.5221	0.8019	0.3614	0.1047	0.2814	0.2567	0.0800
18	0.4310	0.7178	0.4616	0.1534	0.3513	0.3082	0.1103
19	0.9692	0.8179	0.1099	0.0958	0.0155	0.0141	0.0944
20	0.7197	0.7160	0.2863	0.1545	0.1522	0.1318	0.1341
21	0.5979	0.7064	0.3584	0.1603	0.2289	0.1981	0.1295
22	0.9828	0.7176	0.1609	0.1535	0.0086	0.0074	0.1523
23	0.7239	0.7399	0.2717	0.1403	0.1498	0.1314	0.1220
24	0.5542	0.7608	0.3589	0.1282	0.2586	0.2308	0.1004
25	1.0000	0.6980	0.1653	0.1653	0.0000	0.0000	0.1653
26	0.7220	0.8423	0.2221	0.0823	0.1509	0.1398	0.0712
27	0.5911	0.6819	0.3745	0.1751	0.2334	0.1994	0.1411

3.2 Determine weight

The weight for every criterion must be determined to select the optimal case. In this work, the MEREC method was applied to determine the weight. The MEREC method, as presented in Section 2.4, and Eqs. (3)-(8) results were listed in Table 3. Column 2nd was the result of H_{ij} values for output displacement when Eq. (3) was used for calculating, and column 3rd was the result of H_{ij} values for output maximum principal stress when Eq. (4) was used for calculating. Column 4th was the result of S_i values when Eq. (5) was used for calculation.

Columns 5th and 6th were the result of S_{ij} 's values for output displacement and output maximum principal stress when Eq. (6) was used for calculating. Columns 7th and 8th resulted from e_j values for output displacement and output maximum principal stress when Eq. (7) was used for calculation. Finally, the weight results obtained for the two criteria of displacement were 0.7633 and stress were 0.2367 when Eq. (8) was used for calculation.

3.3 Grey relational analysis

Grey theory was frequently applied to systems with unclear

models or incomplete knowledge [28]. Using a large number of discrete inputs, this effectively addressed the uncertainty problem [29].

GRA, a component of gray systems theory, is appropriate for solving numerous factors [30, 31], as follows:

Step 1: Determine the values of the objective

The largest value is the optimal in Eq. (9), and the smallest value is optimal in Eq. (10).

$$D_i^* = \frac{D_i^{(0)}(k) - \min D_i^0(k)}{\max D_i^{(0)}(k) - \min D_i^{(0)}(k)} \quad (9)$$

$$D_i^* = \frac{\max D_i^{(0)}(k) - D_i^0(k)}{\max D_i^{(0)}(k) - \min D_i^{(0)}(k)} \quad (10)$$

where, $D_i^{(0)}(k)$ are the values of D_i and S_i obtained from the method mentioned in Section 2.2.

Step 2: Calculate deviation

$$\Delta_{0i} = \|D_0^*(k) - D_i^*(k)\| \quad (11)$$

$$\Delta_{\min} = \max_{\forall j \in i} \min_{\forall k} \|D_0^*(k) - D_j^*(k)\| \quad (12)$$

$$\Delta_{\max} = \max_{\forall j \in i} \max_{\forall k} \|D_0^*(k) - D_j^*(k)\| \quad (13)$$

Step 3: Estimate the grey relational coefficient (GRC) (γ)

$$\gamma_i(k) = \frac{\Delta_{\min} + \xi \Delta_{\max}}{\Delta_{0i} + \xi \Delta_{\max}} \quad (14)$$

where, $\xi = 0.5$.

Step 4: Compute GRG (ψ_i)

$$\psi_i = \sum_{k=1}^n w_k \gamma_i(k) \quad (15)$$

where, n is the total of the test and w_k is the weight of each objective obtained by the MEREC method.

Step 5: Compute the rank of the GRG value. The highest value of GRG was ranked first in the optimal case.

Table 4. Results of the grey relational analysis

Experiment No.	$D_i^*(1)$	$D_i^*(2)$	$\Delta_{oi}(1)$	$\Delta_{oi}(2)$	$\gamma_i(1)$	$\gamma_i(2)$	ψ_i	Rank
1	0.5083	0.0000	0.4917	1.0000	0.5042	0.3333	0.4637	13
2	0.7872	0.0971	0.2128	0.9029	0.7014	0.3564	0.6197	2
3	1.0000	0.4163	0.0000	0.5837	1.0000	0.4614	0.8725	1
4	0.4597	0.1429	0.5403	0.8571	0.4806	0.3684	0.4540	16
5	0.7369	0.4600	0.2631	0.5400	0.6552	0.4808	0.6139	4
6	0.5638	0.7054	0.4362	0.2946	0.5341	0.6293	0.5566	5
7	0.4183	0.4314	0.5817	0.5686	0.4622	0.4679	0.4635	14
8	0.3417	0.7973	0.6583	0.2027	0.4317	0.7115	0.4979	9
9	0.5020	1.0000	0.4980	0.0000	0.5010	1.0000	0.6191	3
10	0.2178	0.2881	0.7822	0.7119	0.3900	0.4126	0.3953	25
11	0.3887	0.4876	0.6113	0.5124	0.4499	0.4939	0.4603	15
12	0.5081	0.6386	0.4919	0.3614	0.5041	0.5805	0.5222	6
13	0.2001	0.4410	0.7999	0.5590	0.3846	0.4721	0.4053	24
14	0.3657	0.5899	0.6343	0.4101	0.4408	0.5494	0.4665	12
15	0.4381	0.4797	0.5619	0.5203	0.4709	0.4901	0.4754	11
16	0.1831	0.6144	0.8169	0.3856	0.3797	0.5646	0.4235	23
17	0.2628	0.5799	0.7372	0.4201	0.4041	0.5434	0.4371	20
18	0.3791	0.8261	0.6209	0.1739	0.4461	0.7420	0.5161	7
19	0.0091	0.5333	0.9909	0.4667	0.3354	0.5172	0.3784	27
20	0.1118	0.8315	0.8882	0.1685	0.3602	0.7480	0.4520	17
21	0.1931	0.8597	0.8069	0.1403	0.3826	0.7808	0.4769	10
22	0.0050	0.8267	0.9950	0.1733	0.3345	0.7427	0.4311	22
23	0.1095	0.7616	0.8905	0.2384	0.3596	0.6772	0.4348	21
24	0.2310	0.7004	0.7690	0.2996	0.3940	0.6253	0.4488	18
25	0.0000	0.8841	1.0000	0.1159	0.3333	0.8118	0.4466	19
26	0.1106	0.4617	0.8894	0.5383	0.3599	0.4816	0.3887	26
27	0.1986	0.9312	0.8014	0.0688	0.3842	0.8790	0.5013	8

The results of Eqs. (9)-(15) were presented in Table 4 and were archived by substituting the obtained D_i and S_i values from Table 2, where $D_i^*(1)$ and $D_i^*(2)$ are the values of the objective functions in which a larger displacement is better, and the smaller stress is better, respectively; $\Delta_{oi}(1)$ and $\Delta_{oi}(2)$ are the deviation values of the two criteria; and $\gamma_i(1)$ and $\gamma_i(2)$ are the grey relational coefficients of two criteria. Finally, ψ_i represents the GRG values. The optimal case was obtained by ranking the GRG values according to the criterion that the highest GRG value is the best. Therefore, the third case is the optimum case with the design variable at $T_1L_1D_3R_3$.

3.4 TOPSIS method

With multi-objective optimization problem was achieving high amplification while minimizing stress. The TOPSIS approach [32, 33] was used to confirm the optimal stress and displacement values of the innovative BT amplifier, as follows:

Step 1: Determine the objective's normalized values.

$$n_{ij} = \frac{u_{ij}}{\sqrt{\sum_{i=1}^n u_{ij}^2}} \quad (16)$$

where, u_{ij} are the values of D_i and S_t obtained from the method mentioned in Section 2.2.

Step 2: Determine the objective's weighted normalized values.

$$v_{ij} = w_i n_{ij} \tag{17}$$

where, w_i is the weight of each objective obtained by the MEREC method.

Step 3: Calculate the highest and lowest values of v_{ij}

$$v^+ = (v_1^+, v_2^+, \dots, v_n^+) \tag{18}$$

$$v^- = (v_1^-, v_2^-, \dots, v_n^-) \tag{19}$$

Step 4: Determine values K_i^+ and K_i^- of the optimal criteria

$$K_i^+ = \sqrt{\sum_{j=1}^n (v_{ij} - v_j^+)^2} \tag{20}$$

$$K_i^- = \sqrt{\sum_{j=1}^n (v_{ij} - v_j^-)^2} \tag{21}$$

Step 5: Determine the values of CC_i

$$CC_i = \frac{K_i^-}{K_i^+ + K_i^-} \tag{22}$$

Step 6: Calculate the highest value of the CC_i ranked first, which is the optimal case.

Using Eqs. (16)-(19) of the TOPSIS method to calculate the maximum and minimum values of the objective function, Table 5 shows the calculated results. The values of K_i^+ and K_i^- were determined using Eqs. (20)-(21). The CC_i values were then calculated using Eq. (22). The largest value of CC_i was ranked as the third case, indicating that the third instance was the best. The optimal CC_i value obtained was 0.9508. Twenty-seven CC_i values were not identical. This difficulty so implies that the intended variables had a considerable effect on output displacement and stress. This result is identical to that discovered via Grey-R-A and FEA.

Table 5. Results of the TOPSIS method

Experiment No.	n_{ij}		V_{ij}		K_i^+	K_i^-	CC_i	Rank
	D_i	S_t	D_i	S_t				
1	0.2272	0.2391	0.1734	0.0566	0.1089	0.1108	0.5043	7
2	0.3069	0.2312	0.2342	0.0547	0.0496	0.1716	0.7759	2
3	0.3677	0.2051	0.2806	0.0485	0.0113	0.2182	0.9508	1
4	0.2133	0.2274	0.1628	0.0538	0.1190	0.1003	0.4573	8
5	0.2925	0.2015	0.2233	0.0477	0.0583	0.1609	0.7340	3
6	0.2431	0.1815	0.1855	0.0430	0.0953	0.1237	0.5649	4
7	0.2015	0.2038	0.1538	0.0483	0.1273	0.0916	0.4184	10
8	0.1796	0.1740	0.1371	0.0412	0.1436	0.0761	0.3463	14
9	0.2254	0.1574	0.1721	0.0373	0.1086	0.1112	0.5059	6
10	0.1442	0.2156	0.1101	0.0510	0.1711	0.0478	0.2184	17
11	0.1931	0.1993	0.1474	0.0472	0.1336	0.0853	0.3895	11
12	0.2272	0.1869	0.1734	0.0443	0.1075	0.1115	0.5092	5
13	0.1392	0.2031	0.1062	0.0481	0.1747	0.0444	0.2028	20
14	0.1865	0.1909	0.1423	0.0452	0.1385	0.0805	0.3676	13
15	0.2072	0.1999	0.1581	0.0473	0.1229	0.0960	0.4385	9
16	0.1343	0.1889	0.1025	0.0447	0.1782	0.0417	0.1894	21
17	0.1571	0.1917	0.1199	0.0454	0.1609	0.0584	0.2662	15
18	0.1903	0.1716	0.1453	0.0406	0.1354	0.0842	0.3834	12
19	0.0846	0.1955	0.0646	0.0463	0.2162	0.0105	0.0463	27
20	0.1140	0.1712	0.0870	0.0405	0.1937	0.0292	0.1310	22
21	0.1372	0.1689	0.1047	0.0400	0.1759	0.0453	0.2046	19
22	0.0835	0.1716	0.0637	0.0406	0.2169	0.0160	0.0688	26
23	0.1133	0.1769	0.0865	0.0419	0.1942	0.0281	0.1262	23
24	0.1480	0.1819	0.1130	0.0431	0.1678	0.0521	0.2371	16
25	0.0820	0.1669	0.0626	0.0395	0.2180	0.0171	0.0727	25
26	0.1136	0.2014	0.0867	0.0477	0.1942	0.0257	0.1169	24
27	0.1388	0.1630	0.1059	0.0386	0.1747	0.0469	0.2116	18

3.5 SAW method

To improve the dependability of the GRA and TOPSIS approaches, the SAW (Simple Additive Weighting) method, which is extensively used in decision making for multi-objective issues [34]. In this study, the confirmation of the optimal values of the D_i and the S_t was performed using the SAW method [35] as follows:

Step 1: Determine the normalized values of each criterion

The largest value is the optimal in Eq. (23), and the smallest value is optimal in Eq. (24).

$$n_{ij} = \frac{u_{ij}}{\max u_{ij}} \tag{23}$$

$$n_{ij} = \frac{\min u_{ij}}{u_{ij}} \tag{24}$$

where, u_{ij} are the values of D_i and S_t obtained from the method mentioned in Section 2.2.

Step 2: Determine the sum of the weight-normalized values

$$v_i = \sum_{j=1}^n w_j \cdot n_{ij} \quad (25)$$

where, w_j is the weight of each objective obtained by the MEREC method.

Step 3: Calculate the highest value of the v_i ranked first, which is the optimal case.

Table 6. Results of the SAW method

Experiment No.	n_{ij}		V_i	Rank
	D_i	S_t		
1	0.61795	0.65843	0.62753	7
2	0.83466	0.68101	0.79829	2
3	1.00000	0.76757	0.94498	1
4	0.58020	0.69222	0.60671	10
5	0.79560	0.78118	0.79219	3
6	0.66114	0.86744	0.70997	4
7	0.54808	0.77222	0.60114	11
8	0.48854	0.90485	0.58709	13
9	0.61313	1.00000	0.70471	5
10	0.39231	0.73029	0.47232	21
11	0.52509	0.79001	0.58780	12
12	0.61787	0.84213	0.67096	6
13	0.37853	0.77519	0.47243	20
14	0.50717	0.82457	0.58231	14
15	0.56349	0.78747	0.61651	8
16	0.36537	0.83329	0.47614	19
17	0.42726	0.82107	0.52048	15
18	0.51765	0.91726	0.61225	9
19	0.23017	0.80507	0.36626	27
20	0.30996	0.91962	0.45428	22
21	0.37311	0.93214	0.50545	18
22	0.22699	0.91753	0.39046	26
23	0.30817	0.88995	0.44589	23
24	0.40252	0.86550	0.51211	17
25	0.22308	0.94327	0.39357	25
26	0.30899	0.78171	0.42089	24
27	0.37740	0.96552	0.51662	16

Table 6 displays all of the SAW method's outcomes. The values in columns 2 and 3 were computed using Eqs. (23)-(24). The values of V_i were calculated using Eq. (25). The case with the highest V_i value was ranked third, indicating that it was the best. The ideal V_i value was 0.94498. Twenty-seven V_i values did not match. This difficulty indicates that the planned variables had a significant impact on output displacement and stress.

This result is identical to that found via gray relational analysis, finite element analysis, and the TOPSIS method.

3.6 WASPAS method

Furthermore, optimum findings were produced utilizing the WASPAS approach [36, 37]. WASPAS is also among the best methods for determining decision procedures for discovering the optimal situation that fulfills numerous criteria or objectives. It was completed as follows:

Step 1: Use Eq. (23) and Eq. (24) to determine n_{ij} ; next determine v_{ij} , Q_i and P_i

$$v_{ij} = w_j \cdot n_{ij} \quad (26)$$

where, w_j is the weight of each objective, obtained by the MEREC method.

$$Q_i = \sum_{j=1}^n v_{ij} \quad (27)$$

$$P_i = \prod_{j=1}^n (v_{ij})^{w_j} \quad (28)$$

Step 2: Determine A_i

$$A_i = \lambda \cdot Q_i + (1 - \lambda) \cdot P_i \quad (29)$$

Step 3: Calculate the highest value of the A_i ranked as the first, which is the optimal case.

Table 7. Results of the WASPAS method

Experiment No.	n_{ij}		v_{ij}		Q_i	P_i	A_i	Rank
	D_i	S_t	D_i	S_t				
1	0.6180	0.6584	0.4717	0.1559	0.6275	0.3629	0.6011	7
2	0.8347	0.6810	0.6371	0.1612	0.7983	0.4602	0.7645	2
3	1.0000	0.7676	0.7633	0.1817	0.9450	0.5434	0.9048	1
4	0.5802	0.6922	0.4429	0.1639	0.6067	0.3500	0.5810	10
5	0.7956	0.7812	0.6073	0.1849	0.7922	0.4583	0.7588	3
6	0.6611	0.8674	0.5046	0.2053	0.7100	0.4079	0.6798	4
7	0.5481	0.7722	0.4183	0.1828	0.6011	0.3439	0.5754	11
8	0.4885	0.9048	0.3729	0.2142	0.5871	0.3270	0.5611	13
9	0.6131	1.0000	0.4680	0.2367	0.7047	0.3983	0.6741	5
10	0.3923	0.7303	0.2994	0.1729	0.4723	0.2629	0.4514	20
11	0.5251	0.7900	0.4008	0.1870	0.5878	0.3346	0.5625	12
12	0.6179	0.8421	0.4716	0.1994	0.6710	0.3846	0.6423	6
13	0.3785	0.7752	0.2889	0.1835	0.4724	0.2595	0.4511	21
14	0.5072	0.8246	0.3871	0.1952	0.5823	0.3292	0.5570	14
15	0.5635	0.7875	0.4301	0.1864	0.6165	0.3529	0.5901	8
16	0.3654	0.8333	0.2789	0.1973	0.4761	0.2569	0.4542	19
17	0.4273	0.8211	0.3261	0.1944	0.5205	0.2885	0.4973	15
18	0.5176	0.9173	0.3951	0.2171	0.6122	0.3429	0.5853	9
19	0.2302	0.8051	0.1757	0.1906	0.3663	0.1791	0.3475	27
20	0.3100	0.9196	0.2366	0.2177	0.4543	0.2320	0.4320	22
21	0.3731	0.9321	0.2848	0.2207	0.5054	0.2681	0.4817	18
22	0.2270	0.9175	0.1733	0.2172	0.3905	0.1828	0.3697	26
23	0.3082	0.8899	0.2352	0.2107	0.4459	0.2292	0.4242	23
24	0.4025	0.8655	0.3072	0.2049	0.5121	0.2791	0.4888	17

25	0.2231	0.9433	0.1703	0.2233	0.3936	0.1816	0.3724	25
26	0.3090	0.7817	0.2358	0.1850	0.4209	0.2227	0.4011	24
27	0.3774	0.9655	0.2881	0.2286	0.5166	0.2727	0.4922	16

Table 7 displays all of the WASPAS method's outcomes. The values in columns 4 and 5 were calculated using Eq. (26). Eq. (27) were calculated Q_i's value. Eq. (28) were calculated P_i's value. The A_i values were then determined with Eq. (29). The highest value of A_i was assigned to the third scenario, indicating that it was the best. The ideal A_i value was 0.9048. Twenty-seven A_i values did not match. This difficulty indicates that the planned variables had a significant impact on output displacement and stress.

This result optimally corresponds to the grey relational analysis, the TOPSIS method, and the SAW method.

3.7 VIKOR method

The VIKOR approach [38, 39] confirmed the ideal situation for the four indicated methods. It is assumed that compromise is appropriate for conflict resolution and that the decision maker chooses the closest option to the ideal, therefore the alternatives are examined against all set criteria. This is likewise an effective and dependable multi-objective optimization method, which is carried out through the following steps:

Step 1: Calculate the maximum and minimum value of each criterion

$$u_j^+ = \max u_{ij} \quad (30)$$

$$u_j^- = \min u_{ij} \quad (31)$$

where, u_{ij} the values of D_i and S_t are obtained from the method mentioned in Section 2.2.

Step 2: Determine the r_{ij} values

$$r_{ij} = \left(\frac{|u_j^+ - u_{ij}|}{|u_j^+ - u_j^-|} \right) \quad (32)$$

Step 3: Determine the S_i values

$$S_i = \sum_{j=1}^n w_j r_{ij} \quad (33)$$

where, w_j is the weight of each objective obtained by the

MEREC method.

Step 4: Determine the R_i values

$$R_i = \max(w_j r_{ij}) \quad (34)$$

Step 5: Determine the maximum and minimum values of the S_i values and the R_i values

$$S^- = \min(S_i) \quad (35)$$

$$S^+ = \max(S_i) \quad (36)$$

$$R^- = \min(R_i) \quad (37)$$

$$R^+ = \max(R_i) \quad (38)$$

Step 6: Determine the Q_i values

$$Q_i = 0.5(S_i - S^-) / (S^+ - S^-) + 0.5(R_i - R^-) / (R^+ - R^-) \quad (39)$$

Step 7: The best alternative, according to the compromise ranking list, is the first with the lowest with the condition that:

Condition 1:

$$Q_i(2) - Q_i(1) \geq DQ \quad (40)$$

where,

(2) = alternative with the second order in ranking Q_i
(1) = alternative with the best order in ranking Q_i

$$DQ = 1/(m - 1) \quad (41)$$

where, m is the number of alternatives.

Condition 2:

Alternative (1) must be ranked best in S_i and R_i

Table 8 presented all of the VIKOR method's outcomes. The values in columns 4 and 5 were computed using Eqs. (33)-(38). The values of Q_i were determined by using Eq. (39). The lowest value of Q_i was ranked third case when the Q_i value was 0.00000, In this table, the values of S_i, R_i, and Q_i were used to determine the optimal ranking (7th column).

Table 8. Results of the VIKOR method

Experiment No.	r _{ij}		S _i	R _i	Q _i	Rank
	D _i	S _t				
1	0.4917	1.0000	0.6121	0.3753	0.51489	7
2	0.2128	0.9029	0.3762	0.2137	0.22377	3
3	0.0000	0.5837	0.1382	0.1382	0.00000	1
4	0.5403	0.8571	0.6153	0.4124	0.54680	10
5	0.2631	0.5400	0.3286	0.2008	0.18079	2
6	0.4362	0.2946	0.4026	0.3329	0.33724	4
7	0.5817	0.5686	0.5786	0.4440	0.54682	11
8	0.6583	0.2027	0.5505	0.5025	0.57432	13
9	0.4980	0.0000	0.3801	0.3801	0.35948	5
10	0.7822	0.7119	0.7655	0.5970	0.79753	21
11	0.6113	0.5124	0.5879	0.4666	0.57126	12
12	0.4919	0.3614	0.4610	0.3754	0.41126	6

13	0.7999	0.5590	0.7429	0.6106	0.79282	20
14	0.6343	0.4101	0.5813	0.4842	0.58080	14
15	0.5619	0.5203	0.5520	0.4288	0.51648	8
16	0.8169	0.3856	0.7148	0.6235	0.78386	19
17	0.7372	0.4201	0.6621	0.5627	0.69910	15
18	0.6209	0.1739	0.5150	0.4739	0.52713	9
19	0.9909	0.4667	0.8668	0.7563	0.99443	27
20	0.8882	0.1685	0.7178	0.6779	0.82949	22
21	0.8069	0.1403	0.6491	0.6159	0.73271	18
22	0.9950	0.1733	0.8005	0.7594	0.95140	26
23	0.8905	0.2384	0.7361	0.6797	0.84345	23
24	0.7690	0.2996	0.6579	0.5870	0.71565	17
25	1.0000	0.1159	0.7907	0.7633	0.94779	25
26	0.8894	0.5383	0.8063	0.6789	0.89097	24
27	0.8014	0.0688	0.6280	0.6117	0.71483	16

According to Eq. (40):

$$Q_i(2) - Q_i(1) = 0.18079 - 0.000 = 0.18079 > DQ = 0.038461$$

Where: $Q_i(1) = 0.000$ is the alternative with the smallest option in Q_i ranking.

$Q_i(2) = 0.18079$ is the alternative with the 2nd smallest option in Q_i ranking

$$DQ = 1/(27-1) = 0.038461 \text{ (Eq. (41))}$$

And according to Figure 5, the third case is the smallest of S_i , R_i , and Q_i . Therefore, the Q_i values were determined according to the criterion that the lower value is the best. The third case is the optimal case.

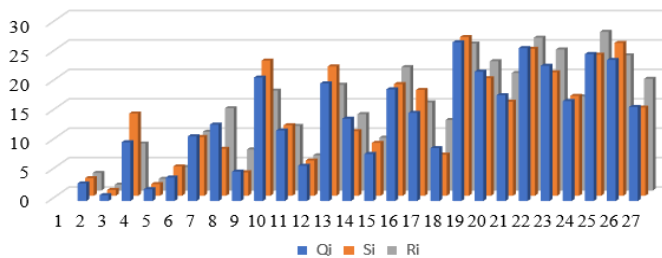


Figure 5. Ranking of Q_i , S_i , and R_i

3.8 Results of signal to noise analysis

The impacts of the levels of the design variables were confirmed by using the Taguchi technique based on the study of S/N. The GRG values and CC_i values in Table 4 and Table 5 were used to analyze S/N. The S/N-A results of GRG and CC_i were listed in Table 9 and Table 10, respectively. The delta values were calculated as the maximum values minus the minimum values. The values in the table revealed that the maximum values are the optimal cases for the design variables. In Table 9, the first rank indicates a variable (T), which significantly affected the GRG value; next is variable (D), a variable (R), and finally, a variable (L). The data from Table 9 was also utilized to generate the graph shown in Figure 6. The levels of the design variables are presented on the horizontal axis, with the S/N values presented on the vertical axis. The variable (T) has a considerable effect on the GRG, next is a variable D, followed by a variable R, and finally by a variable L. The influence grows as the graph's slope increases. In summary, the designed dimensions have a significant influence on the stress and displacement of GMSBTCM. The high peak on the graph indicates that at the position obtained, the optimal levels of the design variables were T1, L1, D3, R3, and that is the third case.

In Table 10, the first rank indicates a variable (T), which significantly affected the CC_i value; next is a variable (D), a

variable (L), and finally a variable (R). The data from Table 10 was also utilized to generate the graph shown in Figure 7. The levels of the design variables are presented on the horizontal axis, with the S/N values presented on the vertical axis. The influence grows as the graph's slope increases. The variable (T) has a considerable effect on the CC_i values; next to is variable D, followed by variable L, and finally by variable R. So, the designed dimensions have a significant influence on the stress and displacement of GMSBTCM. The high peak on the graph indicates that at the position obtained, the optimal levels of the design variables were T1, L1, D3, R3, and that is the third case.

Table 9. Response table for signal to noise ratios of GRG

Level	Thickness (T)	Length (L)	Distance (D)	Radius (R)
1	-5.011	-6.026	-7.370	-7.015
2	-6.863	-6.513	-6.371	-6.190
3	-7.164	-6.501	-5.297	-5.833
Delta	2.153	0.487	2.073	1.182
Rank	1	4	2	3

Table 10. Response table for SN ratios of CC_i

Level	Thickness (T)	Length (L)	Distance (D)	Radius (R)
1	-5.081	-10.442	-14.949	-12.203
2	-10.139	-10.876	-10.751	-11.076
3	-18.528	-12.431	-8.049	-10.470
Delta	13.447	1.988	6.900	1.733
Rank	1	3	2	4

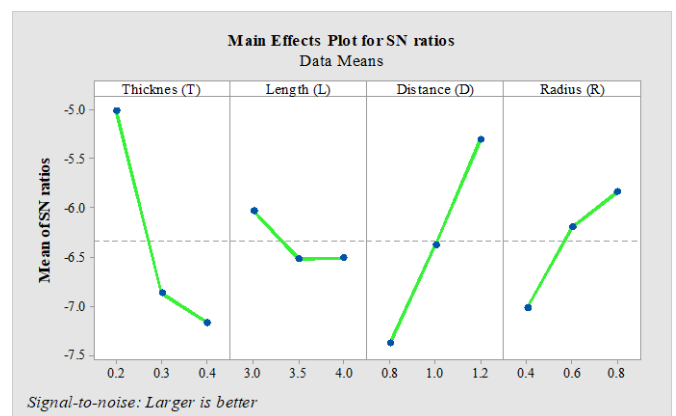


Figure 6. The plot means of S/N of GRG

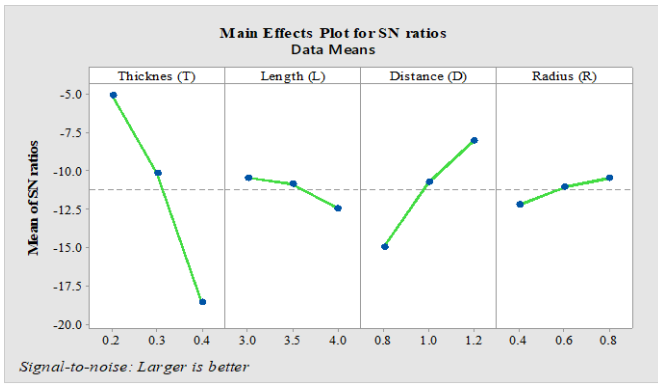


Figure 7. The plot means of S/N of CC_i

Table 11. Response table for signal to noise ratios of V_i

Level	Thickness (T)	Length (L)	Distance (D)	Radius (R)
1	-3.102	-4.733	-6.364	-5.566
2	-5.154	-5.083	-4.997	-5.054
3	-7.095	-5.535	-3.990	-4.732
Delta	3.993	0.802	2.374	0.834
Rank	1	4	2	3

Table 12. Response table for signal to noise ratios of A_i

Level	Thickness (T)	Length (L)	Distance (D)	Radius (R)
1	-3.482	-5.132	-6.780	-5.965
2	-5.545	-5.484	-5.397	-5.459
3	-7.533	-5.944	-4.383	-5.136
Delta	4.051	0.811	2.397	0.829
Rank	1	4	2	3

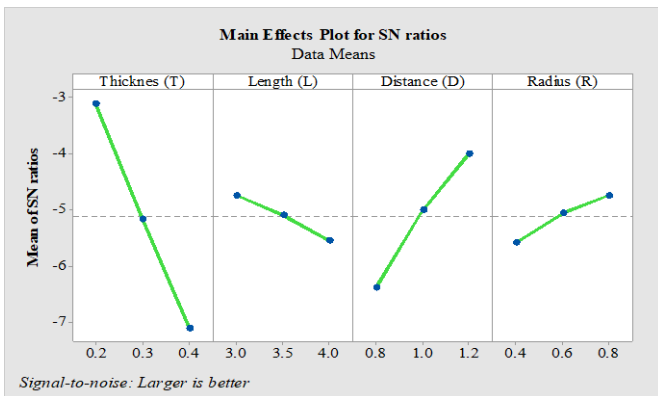


Figure 8. The plot means of S/N of V_i

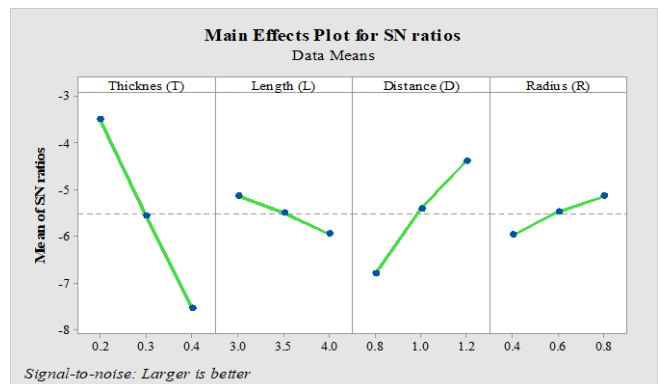


Figure 9. The plot means of S/N of A_i

The impacts of the levels of the design variables were confirmed by using the Taguchi technique based on the study of S/N. The V_i values and A_i values in Table 6 and Table 7 were used to analyze S/N. The S/N-A results of V_i and A_i were listed in Table 11 and Table 12, respectively. The delta values were calculated as the maximum values minus the minimum values. The values in the table revealed that the maximum values are the optimal cases for the design variables. In Tables, the first rank indicates a variable (T), which significantly affected the V_i value and A_i value; next is a variable (D), a variable (R), and finally, a variable (L). The data from this tables were also utilized to generate the graph shown in Figure 8 and Figure 9. The levels of the design variables are presented on the horizontal axis, with the S/N values presented on the vertical axis. The variable T has a considerable effect on the V_i and A_i values; next is a variable D, followed by a variable R, and finally by a variable L. The influence grows as the graph's slope increases. In summary, the designed dimensions have a significant influence on the stress and displacement of GMSBTCM. The high peak on the graph indicates that at the position obtained, the optimal levels of the design variables were T1, L1, D3, R3, and that is the third case.

The results of the analysis of variance (ANOVA) of GRG were presented in Table 13. In this table, column 1 is the designed dimensions and the interaction of the designed dimensions. Column 2 the degree of freedom of the designed dimensions, the interaction of the designed dimensions, and the error. The column 3 is the sequential sum of squares. The column 4 is the contribution percentage of the designed dimensions and the interaction of the designed dimensions. The column 5 is the adjusted sum of squares. The values of column 3 and column 5 are to equal each other. The column 6 is adjusted mean square. Columns 7 and 8 are the F-value and P-value. The F-values are greater than 2 and the P-values are less than 0.05. This indicates that the designed dimensions have strongly affected the GRG, or the displacement and the stress of the GMSBTCM. And the influence of specific design dimensions is as follows: the variable (T) has a considerable effect on the GRG values or the displacement and equivalent stress; next is variable D, followed by variable R, and finally by variable L. This is clearly shown in the percentage contribution column of the design dimensions. In addition, the results of the ANOVA achieved the following R-square, R-square (adjusted), and R-square (pred): values 97.55%, 96.38%, and 95.37%, as presented in Table 14.

The results of the ANOVA analysis of CC_i were presented in Table 15. In this table, column 1 is the designed dimensions and the interaction of the designed dimensions. Column 2: the degree of freedom of the designed dimensions, the interaction of the designed dimensions, and the error. The column 3 is the sequential sum of squares. The column 4 is the contribution percentage of the designed dimensions and the interaction of the designed dimensions. The column 5 is the adjusted sum of squares. The values of the column 3 and column 5 are equal each other. The column 6 is adjusted mean square. Columns 7 and 8 are F-value, and P-value. The F-values are greater than 2 and the P-values are less than 0.05. This indicates that the designed dimensions have strongly affected the CC_i , or the displacement and the stress of the GMSBTCM. And the influence of specific design dimensions is as follows: the variable (T) has a considerable effect on the CC_i values or the displacement and equivalent stress, next is variable D, followed by variable L, and finally by variable R. This is clearly shown in the percentage contribution column of the

design dimensions. In addition, the results of the ANOVA achieved the following R-square, R-square (adjusted), R-

square (pred), values: 99.92%, 99.64%, and 98.34%, as presented in Table 16.

Table 13. Analysis of variance of GRG

Source	DF	Seq SS	Contribution	Adj SS	Adj MS	F-Value	P-Value
T	2	0.095848	36.36%	0.095848	0.047924	44.51	0.000
L	2	0.009124	3.46%	0.009124	0.004562	4.24	0.041
D	2	0.070843	26.87%	0.070843	0.035422	32.90	0.001
R	2	0.026023	9.87%	0.026023	0.013012	12.08	0.008
T*L	4	0.019308	7.32%	0.019308	0.004827	4.48	0.038
T*D	4	0.023188	8.80%	0.023188	0.005797	5.38	0.025
T*R	4	0.012820	4.86%	0.012820	0.003205	2.98	0.073
Error	6	0.006461	2.45%	0.006461	0.001077		
Total	26	0.263617	100.00%				

Table 14. Model summary of GRG

S	R-sq	R-sq(adj)	PRESS	R-sq(pred)	AICc	BIC
0.0328147	97.55%	96.38%	0.130832	95.37%	148.50	-95.99

Table 15. Analysis of variance of CC_i

Source	DF	Seq SS	Contribution	Adj SS	Adj MS	F-Value	P-Value
T	2	0.91338	67.07%	0.913383	0.456692	2448.08	0.000
L	2	0.08302	6.10%	0.083017	0.041509	222.51	0.000
D	2	0.18749	13.77%	0.187492	0.093746	502.52	0.000
R	2	0.03871	2.84%	0.038707	0.019354	103.74	0.000
T*L	4	0.08425	6.19%	0.084246	0.021062	112.90	0.000
T*D	4	0.01021	0.75%	0.010209	0.002552	13.68	0.004
T*R	4	0.04372	3.21%	0.043720	0.010930	58.59	0.000
Error	6	0.00112	0.08%	0.001119	0.000187		
Total	26	1.36189	100.00%				

Table 16. Model summary CC_i

S	R-sq	R-sq(adj)	PRESS	R-sq(pred)	AICc	BIC
0.0136584	99.92%	99.64%	0.0226659	98.34%	101.17	-123.32

Table 17. Analysis of variance of V_i

Source	DF	Seq SS	Contribution	Adj SS	Adj MS	F-Value	P-Value
T	2	0.313625	63.11%	0.313625	0.156813	1785.72	0.000
L	2	0.019667	3.96%	0.019667	0.009833	111.98	0.000
D	2	0.107465	21.62%	0.107465	0.053732	611.88	0.000
R	2	0.018686	3.76%	0.018686	0.009343	106.40	0.000
T*L	4	0.021091	4.24%	0.021091	0.005273	60.04	0.000
T*D	4	0.002849	0.57%	0.002849	0.000712	8.11	0.013
T*R	4	0.013042	2.62%	0.013042	0.003261	37.13	0.000
Error	6	0.000527	0.11%	0.000527	0.000088		
Total	26	0.496953	100.00%				

Table 18. Model summary of V_i

S	R-sq	R-sq(adj)	PRESS	R-sq(pred)	AICc	BIC
0.0093709	99.89%	99.54%	0.0106695	97.85%	80.82	-143.67

The results of the ANOVA analysis of V_i were presented in Table 17. In this table, column 1 is the designed dimensions and the interaction of the designed dimensions. Column 2: the degree of freedom of the designed dimensions, the interaction of the designed dimensions, and the error. The column 3 is the sequential sum of squares. The column 4 is the contribution percentage of the designed dimensions and the interaction of the designed dimensions. The column 5 is the adjusted sum of

squares. The values of column 3 and column 5 are equal to each other. The column 6 is adjusted mean square. Columns 7 and 8 are F-value, and P-value. The F-values are greater than 2 and the P-values are less than 0.05. This indicates that the designed dimensions have strongly affected the V_i, or the displacement and the stress of the GMSBTCM. And the influence of specific design dimensions is as follows: the variable (T) has a considerable effect on the V_i values or the

displacement and equivalent stress, next is variable D, followed by variable L, and finally by variable R. This is clearly shown in the percentage contribution column of the design dimensions. In addition, the results of the ANOVA achieved the following R-square, R-square (adjusted), R-square (pred), values: 99.89%, 99.54%, and 97.85%, as presented in Table 18.

The results of the ANOVA analysis of A_i were presented in Table 19. In this table, column 1 is the designed dimensions, and the interaction of the designed dimensions. Column 2: the degree of freedom of the designed dimensions, the interaction of the designed dimensions, and the error. The column 3 is the sequential sum of square. The column 4 is the contribution percentage of the designed dimensions and the interaction of the designed dimensions. The column 5 is the adjusted sum of

squares. The values of column 3 and column 5 are equal to each other. The column 6 is adjusted mean square. The columns 7 and 8 are F-value, and P-value. The F-values are greater than 2 and the P-values are less than 0.05. This indicates that the designed dimensions have strongly affected the A_i , or the displacement and the stress of the GMSBTCM. And the influence of specific design dimensions is as follows: the variable (T) has a considerable effect on the A_i values or the displacement and the stress, next is variable D, followed by variable L, and finally by variable R. This is clearly shown in the percentage contribution column of the design dimensions. In addition, the results of the ANOVA achieved the following R-square, R-square (adjusted), and R-square (pred), values: 99.9%, 99.56%, and 97.96%, as presented in Table 20.

Table 19. Analysis of variance of A_i

Source	DF	Seq SS	Contribution	Adj SS	Adj MS	F-Value	P-Value
T	2	0.293583	63.41%	0.293583	0.146792	1889.35	0.000
L	2	0.018349	3.96%	0.018349	0.009174	118.08	0.000
D	2	0.099618	21.51%	0.099618	0.049809	641.09	0.000
R	2	0.016989	3.67%	0.016989	0.008494	109.33	0.000
T*L	4	0.019447	4.20%	0.019447	0.004862	62.57	0.000
T*D	4	0.002437	0.53%	0.002437	0.000609	7.84	0.015
T*R	4	0.012139	2.62%	0.012139	0.003035	39.06	0.000
Error	6	0.000466	0.10%	0.000466	0.000078		
Total	26	0.463027	100.00%				

Table 20. Model summary of A_i

S	R-sq	R-sq(adj)	PRESS	R-sq(pred)	AICc	BIC
0.0088144	99.90%	99.56%	0.0094399	97.96%	77.52	-146.97

Table 21. Analysis of variance of Q_i

Source	DF	Seq SS	Contribution	Adj SS	Adj MS	F-Value	P-Value
T	2	1.04863	64.65%	1.04863	0.524316	1396.58	0.000
L	2	0.05282	3.26%	0.05282	0.026410	70.35	0.000
D	2	0.36754	22.66%	0.36754	0.183772	489.50	0.000
R	2	0.05705	3.52%	0.05705	0.028523	75.97	0.000
T*L	4	0.04865	3.00%	0.04865	0.012161	32.39	0.000
T*D	4	0.00868	0.54%	0.00868	0.002171	5.78	0.030
T*R	4	0.03634	2.24%	0.03634	0.009084	24.20	0.001
Error	6	0.00225	0.14%	0.00225	0.000375		
Total	26	1.62196	100.00%				

Table 22. Model summary of Q_i

S	R-sq	R-sq(adj)	PRESS	R-sq(pred)	AICc	BIC
0.0193760	99.86%	99.40%	0.0456146	97.19%	120.05	-104.44

The results of the ANOVA analysis of Q_i were presented in Table 21. In this table, column 1 is the designed dimensions and the interaction of the designed dimensions. Column 2: the degree of freedom of the designed dimensions, the interaction of the designed dimensions, and the error. The column 3 is the sequential sum of squares. The column 4 is the contribution percentage of the designed dimensions and the interaction of the designed dimensions. The column 5 is the adjusted sum of squares. The values of column 3 and column 5 are equal to each other. The column 6 is adjusted mean square. The columns 7 and 8 are F-value, and P-value. The F-values are greater than 2 and the P-values are less than 0.05. This

indicates that the designed dimensions have strongly affected the Q_i , or the displacement and equivalent stress of the GMSBTCM. And the influence of specific design dimensions is as follows: the variable (T) has a considerable effect on the Q_i values or the displacement and equivalent stress, next is variable D, followed by variable R, and finally by variable L. This is clearly shown in the percentage contribution column of the design dimensions. In addition, the results of the ANOVA achieved the following R-square, R-square (adjusted), and R-square (pred) values: 99.86%, 99.4%, and 97.19%, as presented in Table 22. Through the R-square of the ANOVA analysis results of GRG, CC_i , V_i , A_i , and Q_i , it was shown that

the ANOVA analysis results showed that the best result was the TOPSIS method, next to is the WASPAS method, SAW method, VIKOR method, and finally the grey relational analysis.

3.9 Discussion of optimization methods

Table 23 provides a synthesis of the optimal rankings of the five implemented methods. The Saw and Waspas methods yield very similar ranking results in this table. There are only two cases: Case 10 is ranked 21 with the SAW method and 20 with the WASPAS method, while Case 13 is the opposite, with the Saw method ranking at 20 and Waspas at 21. These two methods share similarities in their calculations, yielding almost identical results. Generally, all 5 methods rank Case 3 as the best optimal and Case 19 as the badest optimal (rank 27). Cases 2, 12, 17, 22, 23, and 25 have 4 methods with identical rankings; the remaining cases differ between the two methods.

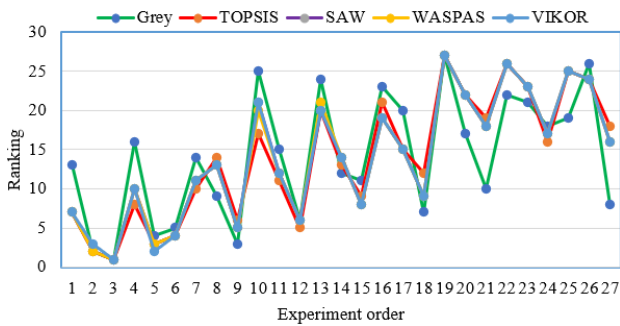


Figure 10. The optimal result of ranking

The similarity in rankings is shown in Figure 10 when the ranking lines of the five methods have the same similarity and look in the same direction.

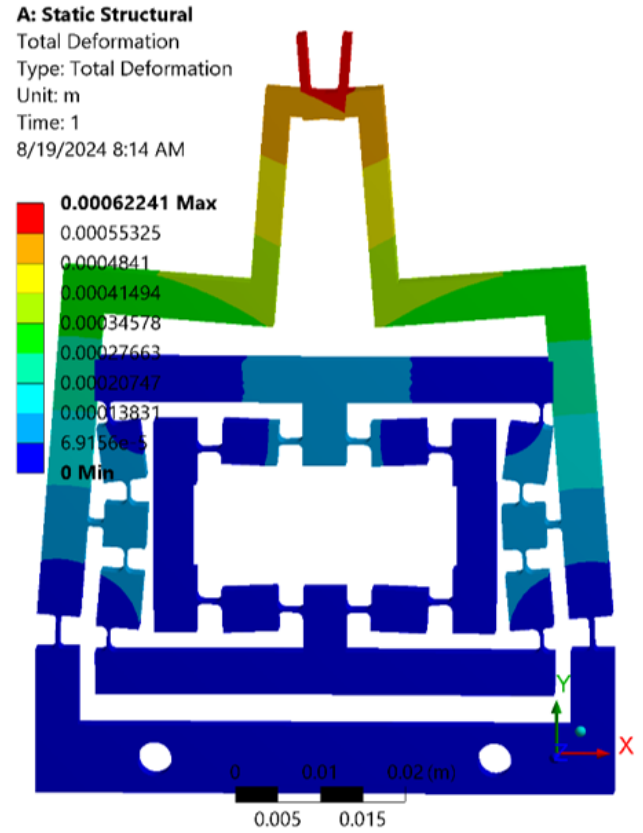


Figure 11. The result of output displacement

Table 23. The optimal result of ranking

Experiment No.	Ranking				
	Grey	TOPSIS	SAW	WASPAS	VIKOR
1	13	7	7	7	7
2	2	2	2	2	3
3	1	1	1	1	1
4	16	8	10	10	10
5	4	3	3	3	2
6	5	4	4	4	4
7	14	10	11	11	11
8	9	14	13	13	13
9	3	6	5	5	5
10	25	17	21	20	21
11	15	11	12	12	12
12	6	5	6	6	6
13	24	20	20	21	20
14	12	13	14	14	14
15	11	9	8	8	8
16	23	21	19	19	19
17	20	15	15	15	15
18	7	12	9	9	9
19	27	27	27	27	27
20	17	22	22	22	22
21	10	19	18	18	18
22	22	26	26	26	26
23	21	23	23	23	23
24	18	16	17	17	17
25	19	25	25	25	25
26	26	24	24	24	24
27	8	18	16	16	16

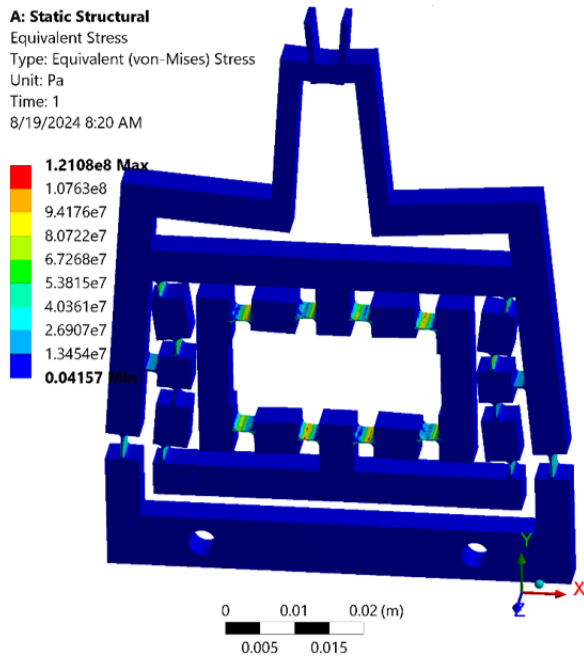


Figure 12. The result of maximum principal stress

Figure 11 is the result of the displacement and Figure 12 is the result of max stress representing the optimal rankings of the 5 methods. The grey relational analysis method exhibits larger differences than the other methods, as indicated by its more distinct representation line than the others. The remaining methods show relatively insignificant variations in rankings. Specifically, Case 3 is the optimal case for all 5 methods, while Case 19 is the badest case, demonstrated by all 5 representation lines converging to one point. This reflects the similarity among the methods. The case with inconsistent ranking results among the 5 methods is Case 10, where almost four optimal methods share a different ranking. From these results, it can be inferred that the optimization methods exhibit similarity with each other and do not differ significantly in results.

4. CONCLUSIONS

This research can be concluded as follows. Firstly, 27 models were designed by SolidWorks based on an experimental design by Minitab. Next, ANSYS was used in this work to create and analyze the finite element model of 27 models to determine the displacement and the maximum principal stress. The outcomes of the FEM indicated that the design parameters strongly affect the displacement and maximum principal stress because the outcomes of the 27 cases changed significantly. An analysis of S/N was done to examine and validate the FEA model. The outcomes of all of the models showed that the T variable of FH has the greatest influence, followed by the D value, the L value, and finally, R. The optimal case was determined using the multi-objective optimization method of GRA based on the weight MEREC method. Finally, the optimal case was determined to be the third case by GRA, and four multi-objective optimization methods were applied to confirm this result. Therefore, five multi-objective optimization methods all concluded that the third case is optimal, with the combination design variables at $T_1L_1D_3R_3$. The optimal case had 0.62241 mm of output displacement and 121.08 MPa of the maximum principal

stress, respectively. In this case, the thickness of the flexure hinge was 0.2 mm, the length of the FH was 3 mm, the distance between the centers of the two FHs was 1.2 mm, and the radius between the rigid link and FHs was 0.8 mm. TOPSIS, SAW, WASPAS, and VIKOR techniques all demonstrate that case 3 was the best. According to these approaches; the 19th case had the lowest rank, which corresponds to the 0.14326 mm of output displacement and 115.44 MPa of the maximum principal stress; the thickness of the FH was 0.4 mm, the length of the FH was 3 mm, the distance between the centers of the two FHs was 0.8 mm, and the radius between the rigid link and FHs was 0.4 mm. Based on the study's exceptional results, the authors will re-examine several hypotheses to optimize the model structure for building a micro-detailed clamping mechanism in structural and plant biology research.

REFERENCES

- [1] Wang, Y.L., Jin, K., Chang, L., Pan, H.M., Cao, F.F., Xu, Z.K. (2024). Research on the measurement mechanism of a six-axis force sensor based on a flexible hinge series-parallel hybrid. *Measurement Science and Technology*, 35: 126012. <https://doi.org/10.1088/1361-6501/ad78f4>
- [2] Chen, W.H., Wang, R.C., Liu, K. (2024). Active compliant mechanisms for optimized actuation by LCE-based artificial muscles. *Mechanics of Materials*, 189: 1-11. <https://doi.org/10.1016/j.mechmat.2023.104879>
- [3] Chen, X.D., Xie, Z.M., Tai, K., Tan, H.F. (2024). Design of low parasitic motion microgripper based on symmetrical parallelogram mechanism. *Sensors and Actuators A: Physical*, 367: 115072. <https://doi.org/10.1016/j.sna.2024.115072>
- [4] Das, T.K., Shirinzadeh, B. (2024). Design, computational analysis and experimental study of a high amplification piezoelectric actuated microgripper. *Engineering Research Express*, 6: 035509. <https://doi.org/10.1088/2631-8695/ad5f19>
- [5] de Almeida, B.V., Pavanello, R., Langelaar, M. (2024). Topology optimization of smart structures with embedded piezoelectric stack actuators using a composite geometry projection method. *Computer Methods in Applied Mechanics and Engineering*, 429: 117120. <https://doi.org/10.1016/j.cma.2024.117120>
- [6] Fava, M., Parenti-Castelli, V., Conconi, M., Sancisi, N. (2024). A new combined fabrication process to shape small flexure hinges. *Meccanica* 59: 1327-1334. <https://doi.org/10.1007/s11012-024-01860-9>
- [7] Wang, Y., Zhang, L.Z., Meng, L.X., Lu, H.J., Ma, Y.H. (2024). Theoretical modeling and experimental verification of elliptical hyperbolic hybrid flexure hinges. *Symmetry*, 16(3): 345. <https://doi.org/10.3390/sym16030345>
- [8] Guan, J.H., Deng, J., Zhang, S.J., Liu, J.K., Liu, Y.X. (2024). A spatial 3-DOF piezoelectric robot and its speed-up trajectory based on improved stick-slip principle. *Sensors and Actuators A: Physical*, 374: 115502. <https://doi.org/10.1016/j.sna.2024.115502>
- [9] Hu, J.Y., Wallin, M., Ristinmaa, M., Liu, Y., Liu, S. (2024). Integrated multi-material and multi-scale optimization of compliant structure with embedded movable piezoelectric actuators. *Computer Methods in Applied Mechanics and Engineering*, 421: 116786. <https://doi.org/10.1016/j.cma.2024.116786>

- [10] Jani, N., Tirupathi, R., Menon, P.K., Pandey, A.K. (2024). Modelling and optimization of compound lever-based displacement amplifier in a MEMS accelerometer. *Microsystem Technologies*, 1-20. <https://doi.org/10.1007/s00542-024-05757-1>
- [11] Khurana, M.M., Joglekar, M.M., Motzki, P., Seelecke, S. (2024). Compliant frame geometry for DEMES-based gripper and flapping wing actuators: A comprehensive design study. *International Journal of Solids and Structures*, 30: 112969. <https://doi.org/10.1016/j.ijsolstr.2024.112969>
- [12] Lavanya, S.B., Jayanth, G.R. (2024). A nano-positioning system based on an optimal two-stage linear displacement amplifier. *Sensors and Actuators A: Physical*, 366: 114984. <https://doi.org/10.1016/j.sna.2023.114984>
- [13] Maggie, Y. (2023). Micro Clamp/Wire Clamp/Micro Gripper for Lead Bonding Based on Piezo Ceramics. Harbin Core Tomorrow Science & Technology Co., Ltd. https://www.researchgate.net/publication/369416553_Micro_ClampWire_ClampMicro_Gripper_for_Lead_Bonding_Based_on_Piezo_Ceramics.
- [14] Ghosh, B., Jain, R. (2024). Experimental performance evaluation of shape memory alloy (SMA) compliant micro gripper for micro assembly. *Journal of Scientific & Industrial Research*, 83(9): 1022-1032. <https://doi.org/10.56042/jsir.v83i9.2542>
- [15] Guo, Z.Y., Ma, H.F., Li, Q.H., Li, Y.M., Liu, Z.Q., Song, Q.H. (2023). Design and analysis of a compliant microgripper with a large amplification ratio. *Microsystem Technologies*, 29: 1333-1341. <https://doi.org/10.1007/s00542-023-05505-x>
- [16] Ling, M.X., Yuan, L., Zeng, T.J., Zhang, X.M. (2024). Enabling the transfer matrix method to model serial-parallel compliant mechanisms including curved flexure beams. *International Journal of Mechanical System Dynamics*, 4(1): 48-62. <https://doi.org/10.1002/msd2.12097>
- [17] Zhou, K., Liu, P., Lu, S., Yan, P. (2022). Design and modeling of a piezo-driven three-dimensional bridge-type amplification mechanism with input/output guiding constraint. *Review of Scientific Instruments*, 93(2): 025005. <https://doi.org/10.1063/5.0076287>
- [18] Lyu, Z.K. (2022). Design and testing of a new piezoelectric-actuated symmetric compliant microgripper. *Actuators*, 11(3): 77. <https://doi.org/10.3390/act11030077>
- [19] Chen, X.D., Deng, Z.L., Hu, S.Y., Gao, X.J., Gao, J.H. (2020). Research on three-stage amplified compliant mechanism-based piezo-driven microgripper. *Advances in Mechanical Engineering*, 12(3): 1687814020911470. <https://doi.org/10.1177/1687814020911470>
- [20] Wu, S.L., Ling, M.X., Wang, Y.B., Huang, T. (2024). Electro-mechanical transfer matrix modeling of piezoelectric actuators and application for elliptical flexure amplifiers. *Precision Engineering*, 85: 279-290. <https://doi.org/10.1016/j.precisioneng.2023.10.009>
- [21] Wang, D.S., Zhao, Y.R., Yang, H.M., Hong, K.P. (2024). Closed-loop control of microgripper system based on compliant mechanism. *AIP Advances*, 14: 075227. <https://doi.org/10.1063/5.0206315>
- [22] Wu, Z., Wang, Y., Chen, M., Ding, B. (2024). Design, analysis, and experimental investigations of an asymmetrical under-actuated micro-gripper. *Journal of Intelligent Material Systems and Structures*, 35(11): 960-970. <https://doi.org/10.1177/1045389X241246827>
- [23] Zhang, S., Liu, J., Ding, H., Zhang, Y. (2024). Dynamic modeling and experimental verification of an RPR type compliant parallel mechanism with low orders. *Chinese Journal of Mechanical Engineering*, 37: 78. <https://doi.org/10.1186/s10033-024-01050-4>
- [24] Li, J., Huang, W., Xie, Y., Yang, J., Zhao, M. (2024). The parameters optimization of robotic polishing with force controlled for mold steel based on Taguchi method. *Journal of the Brazilian Society of Mechanical Sciences and Engineering*, 46(5): 313. <https://doi.org/10.1007/s40430-024-04889-9>
- [25] Georgantzinou, S.K., Kastanos, G., Tseni, A.D., Kostopoulos, V. (2024). Efficient optimization of the multi-response problem in the Taguchi method through advanced data envelopment analysis formulations integration. *Computers & Industrial Engineering*, 197: 110618. <https://doi.org/10.1016/j.cie.2024.110618>
- [26] Hassan, T., Khan, O., Khan, M.Z., Kumari, P., Parvez, M., Eqbal, A., Ahamad, T. (2024). Comparative analysis of nano-additives for enhanced photocatalytic hydrogen production: A hybrid approach using MEREC and sensitivity methods. *Nano-Structures & Nano-Objects*, 40: 101353. <https://doi.org/10.1016/j.nanoso.2024.101353>
- [27] Fan, J.P., Lei, T., Wu, M.Q. (2024). MEREC-MABAC method based on cumulative prospect theory for picture fuzzy sets: Applications to wearable health technology devices. *Expert Systems with Applications*, 255: 124749. <https://doi.org/10.1016/j.eswa.2024.124749>
- [28] Gunasekaran, J., Sevvel, P., John Solomon, I., Roy, J.V. (2024). Multi objective optimization of parameters during FSW of AZ80A - AZ31B Mg alloys using grey relational analysis. *Journal of Mechanical Science and Technology*, 38: 4971-4982. <https://doi.org/10.1007/s12206-024-0832-3>
- [29] Singh, G., Pandey, A. (2024) Environmental sustainability integrated supplier selection in electric vehicle supply chains: A grey relational analysis approach. *Environment, Development and Sustainability*. <https://doi.org/10.1007/s10668-024-05294-x>
- [30] George, P., Dev Wins, K.L., Jacob Dhas, D.S.E., Beatrice, B.A., George, P. (2024). A grey relational-Taguchi analysis on high-speed milling of duplex and super duplex stainless steels used in chemical tankers. *International Journal on Interactive Design and Manufacturing*. <https://doi.org/10.1007/s12008-024-02123-3>
- [31] Georgantzinou, S.K., Kastanos, G., Tseni, A.D., Kostopoulos, V. (2024). Efficient optimization of the multi-response problem in the Taguchi method through advanced data envelopment analysis formulations integration, *Computers & Industrial Engineering*, 197: 110618. <https://doi.org/10.1016/j.cie.2024.110618>
- [32] Ccatamayo-Barrios, J.H., Huamán-Román, Y.L., Seminario-Morales, M.V., Flores-Castillo, M.M., Gutiérrez-Gómez, E., Carrillo-De la cruz, L.K., de la Cruz-Girón, K.A. (2023). Comparative analysis of AHP and TOPSIS multi-criteria decision-making methods for mining method selection. *Mathematical Modelling of Engineering Problems*, 10(5): 1665-1674. <https://doi.org/10.18280/mmep.100516>

- [33] Ayyildiz, E., Erdogan, M. (2024). A FERMATEAN fuzzy SWARA-TOPSIS methodology based on SCOR model for autonomous vehicle parking lot selection. *Applied Soft Computing*, 166: 112198. <https://doi.org/10.1016/j.asoc.2024.112198>
- [34] Naibaho, E. (2024). Application of the SAW (Simple Additive Weighting) method in the selection of foundation scholarship recipients at STMIK Mulia Darma. *Jurnal Multimedia Dan Teknologi Informasi (Jatilima)*, 6(2): 102-108. <https://doi.org/10.54209/jatilima.v6i02.558>
- [35] Susilo, J., Wahyuni, E.G. (2024). Comparison of SAW and TOPSIS methods in decision support systems for contraceptive selection. *International Journal Software Engineering and Computer Science (IJSECS)*, 4(2): 792-807. <https://doi.org/10.35870/ijsecs.v4i2.2815>
- [36] Kavimani, V., Gopal, P.M., Ramakrishnan, S.K., Giri, J., Alarifi, A., Sathish, T. (2024). Predictive modelling and optimization of WEDM parameter for Mg–Li alloy using ANN integrated CRITIC-WASPAS approach. *Heliyon*, 10(15): e35194. <https://doi.org/10.1016/j.heliyon.2024.e35194>
- [37] Arslan, Ö., Cebi, S. (2024). A novel approach for multi-criteria decision making: Extending the WASPAS method using decomposed fuzzy sets, *Computers & Industrial Engineering*, 196: 110461. <https://doi.org/10.1016/j.cie.2024.110461>
- [38] Mali, P.R., Vishwakarma, R.J., Isleem, H.F., Khichad, J.S., Patil, R.B. (2024). Performance evaluation of bamboo species for structural applications using TOPSIS and VIKOR: A comparative study. *Construction and Building Materials*, 449: 138307. <https://doi.org/10.1016/j.conbuildmat.2024.138307>
- [39] Ramdani, H., Aoulmi, Z., Louafi, M., Attia, M., Mebarkia, M. (2024). Enhancing sustainability through drilling machine efficiency: A comparative analysis of TOPSIS and VIKOR methods for energy optimization. *International Journal of Computational Methods and Experimental Measurements*, 12(1): 45-52. <https://doi.org/10.18280/ijcmem.120105>